7.0 Examples of μSR studies in superconductivity

7.1 The vortex state and the corresponding field distribution

Superconductivity characteristics:

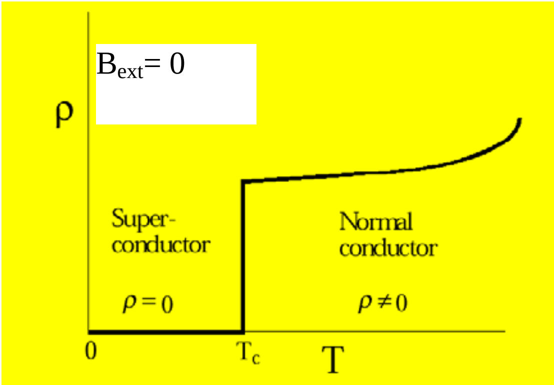

Fig. 7-1: Zero resistance. Resistance versus temperature.

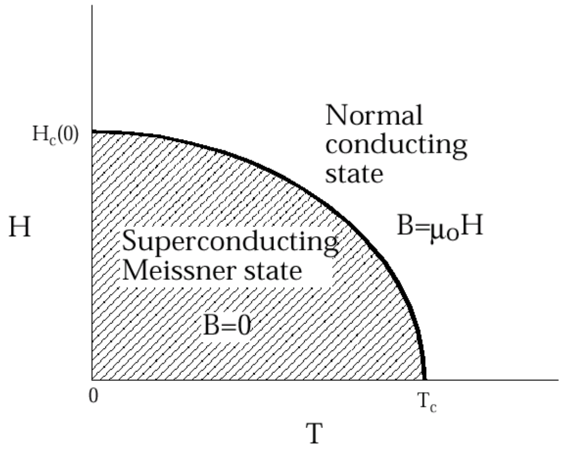

Fig. 7-2: Diamagnetism. Schematic phase diagram of a superconductor of type I, $\kappa \equiv \frac{\lambda}{\xi} < \frac{1}{\sqrt{2}}$.

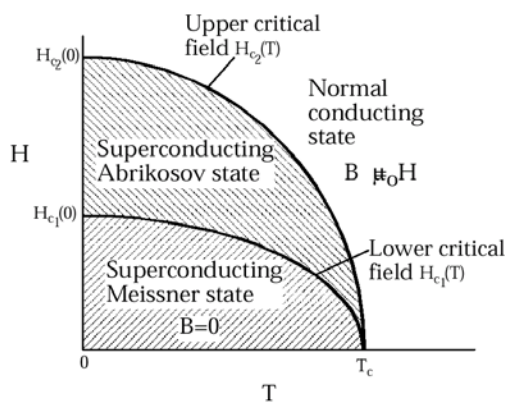

Fig. 7-3: Schematic phase diagram of a superconductor of type II $\kappa \equiv \frac{\lambda}{\xi} > \frac{1}{\sqrt{2}}$.

Superconductors of type II have above H_{c1} a mixed phase, where the magnetic flux can penetrate the sample in the form of fluxoids (vortices). Each vortex contains a flux quantum $\Phi_0 = \frac{h}{2e} = 2.07 \cdot 10^{-15}\ \mathrm{T \cdot m^2}$. The vortices may form a regular lattice, mostly of hexagonal symmetry (flux line lattice, FLL). The FLL is obtained by cooling the superconductor in a field.

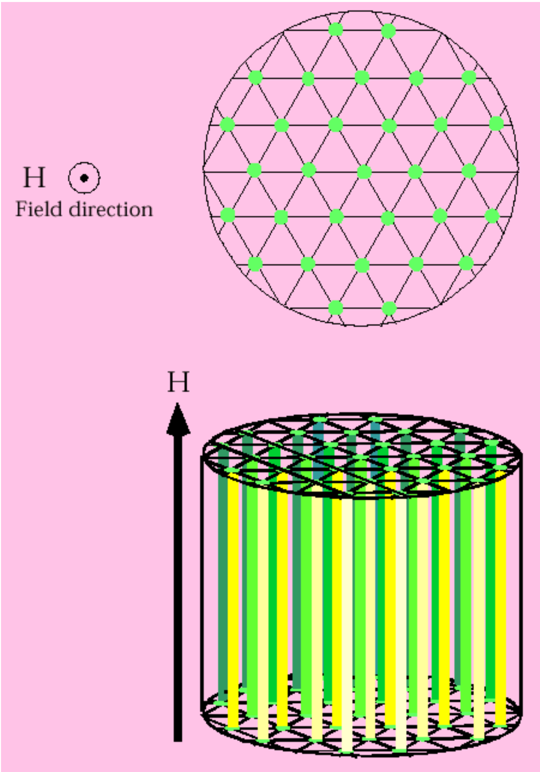

Fig. 7-4: Mixed state (Abrikosov lattice).

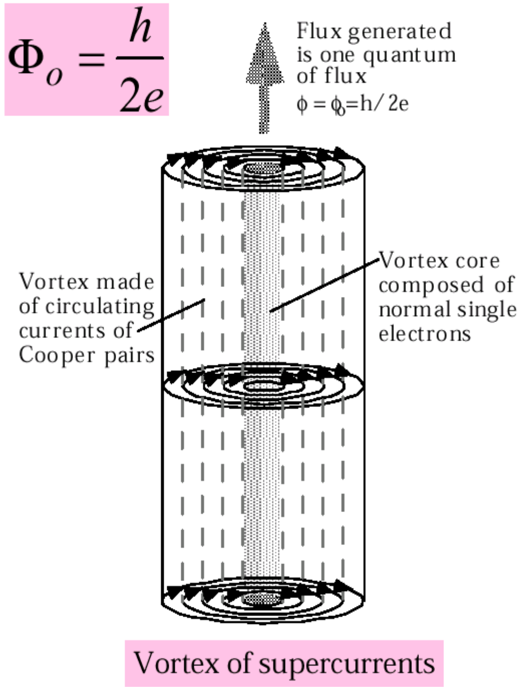

Fig. 7-5: Structure of a vortex

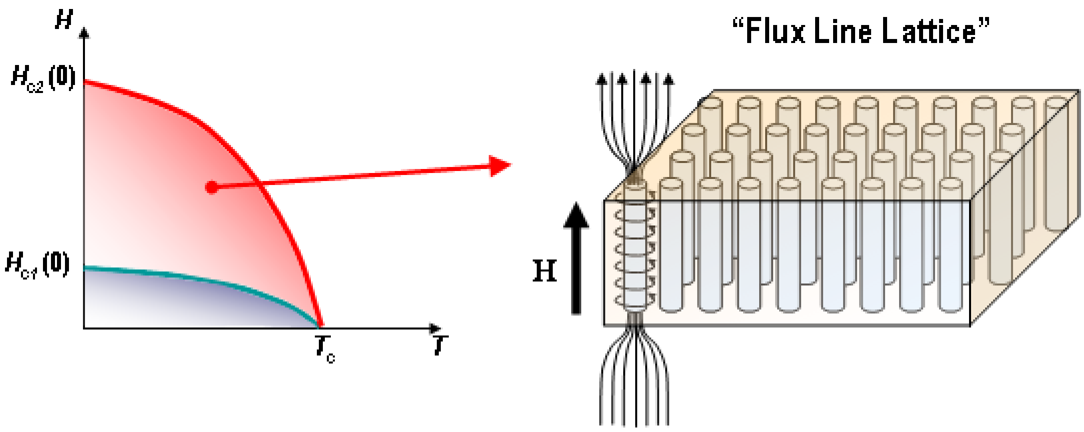

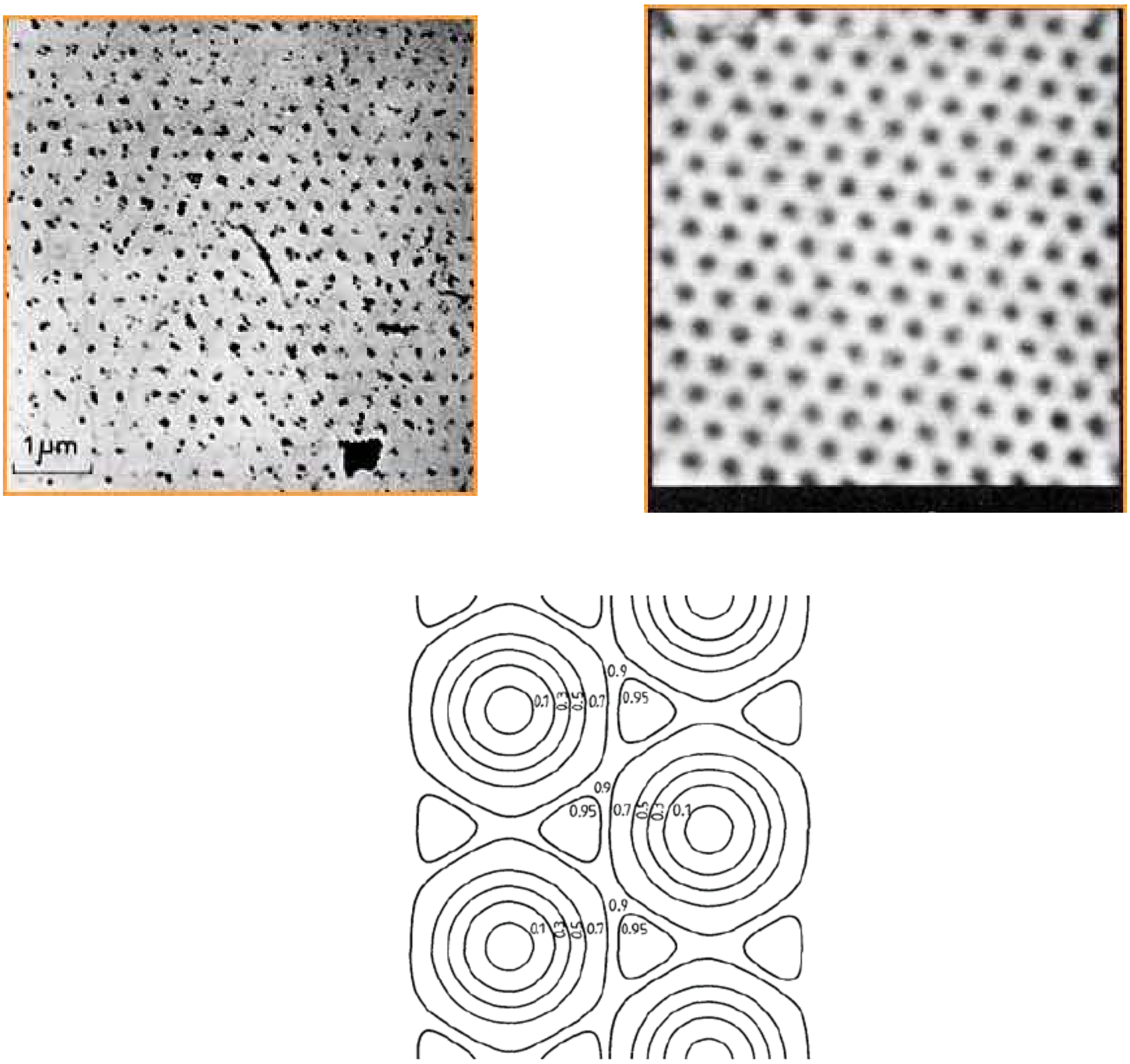

Fig. 7-6: Visualization of a vortex lattice. Top left: Bitter decoration technique. Pb-4at%In, 1.1K, 195 G. (U. Essmann and H. Trauble, Phys. Lett. 24A, 526 (1967)). Top right: Surface image by Scanning Tunnel Microscopy $NbSe_2$, 1T, 1.8K, H. F. Hess et al. Phys. Rev. Lett. 62, 214 (1989) the vortex spacing is ~ 479 Å. Bottom: The hexagonal Abrikosov lattice showing the contour lines.

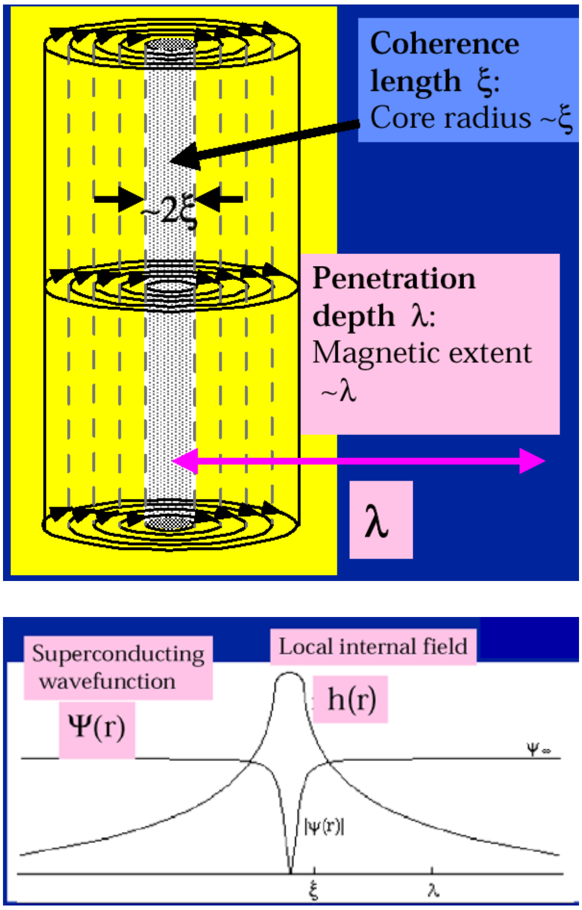

(London) magnetic penetration depth:

Clean limit:

mean free path >> BCS coherence length

$$\ell >> \xi_0 = \frac{\hbar v_F}{\pi \Delta_0}$$

$$\lambda(T) = \sqrt{\frac{m^*}{\mu_0 e^2 n_s(T)}}$$

$\frac{1}{\lambda^2} \propto \frac{n_s}{m^*}$ is called superfluid density

Δ_0 : superconducting gap at T=0

For a clean sc: $n_s(0)=n$

m* : effective mass

n_s : density of the superconducting carriers

n: : carrier density

For a “dirty” superconductor:

$\lambda \rightarrow \lambda\sqrt{1+\frac{\xi_0}{\ell}}$ and the superfluid density is reduced by $\approx \frac{\ell}{\xi_0}$

Fig. 7-7: Characteristic length scales in the vortex state. Order parameter ψ(r) and magnetic field h(r) as a function of distance from the center of an isolated vortex (κ≈8). The order parameter squared is proportional to the density of supercarriers n_s.

The field distribution around a single vortex can be obtained from the London equations[1]:

$$B_v(r) = \frac{\Phi_0}{2\pi\lambda^2} K_0\left(\frac{r}{\lambda}\right) \qquad [7\text{-}1]$$

K_0 is the modified Hankel function zeroth order.

[1] London equations: $\frac{d\vec{j}}{dt} = \frac{1}{\mu_0 \lambda_L^2}\vec{E}(t)$ and $\mathrm{rot}\vec{j} = -\frac{1}{\mu_0 \lambda_L^2}\vec{B}(t)$ describe perfect conductivity and diamagnetic shielding in a superconductor.

This function can be approximated as follows:

$$B_v(r) \rightarrow \frac{\Phi_0}{2\pi\lambda^2}\ln\left(\frac{\lambda}{r}\right) \qquad \text{for } \xi << r << \lambda \qquad [7-2]$$

$$B_v(r) \rightarrow \frac{\Phi_0}{2\pi\lambda^2}\sqrt{\frac{\lambda}{r}}e^{-\frac{r}{\lambda}} \qquad \text{for } r >> \lambda \qquad [7-3]$$

μSR can measure the local magnetic field distribution in the vortex state. Qualitatively, we expect following picture:

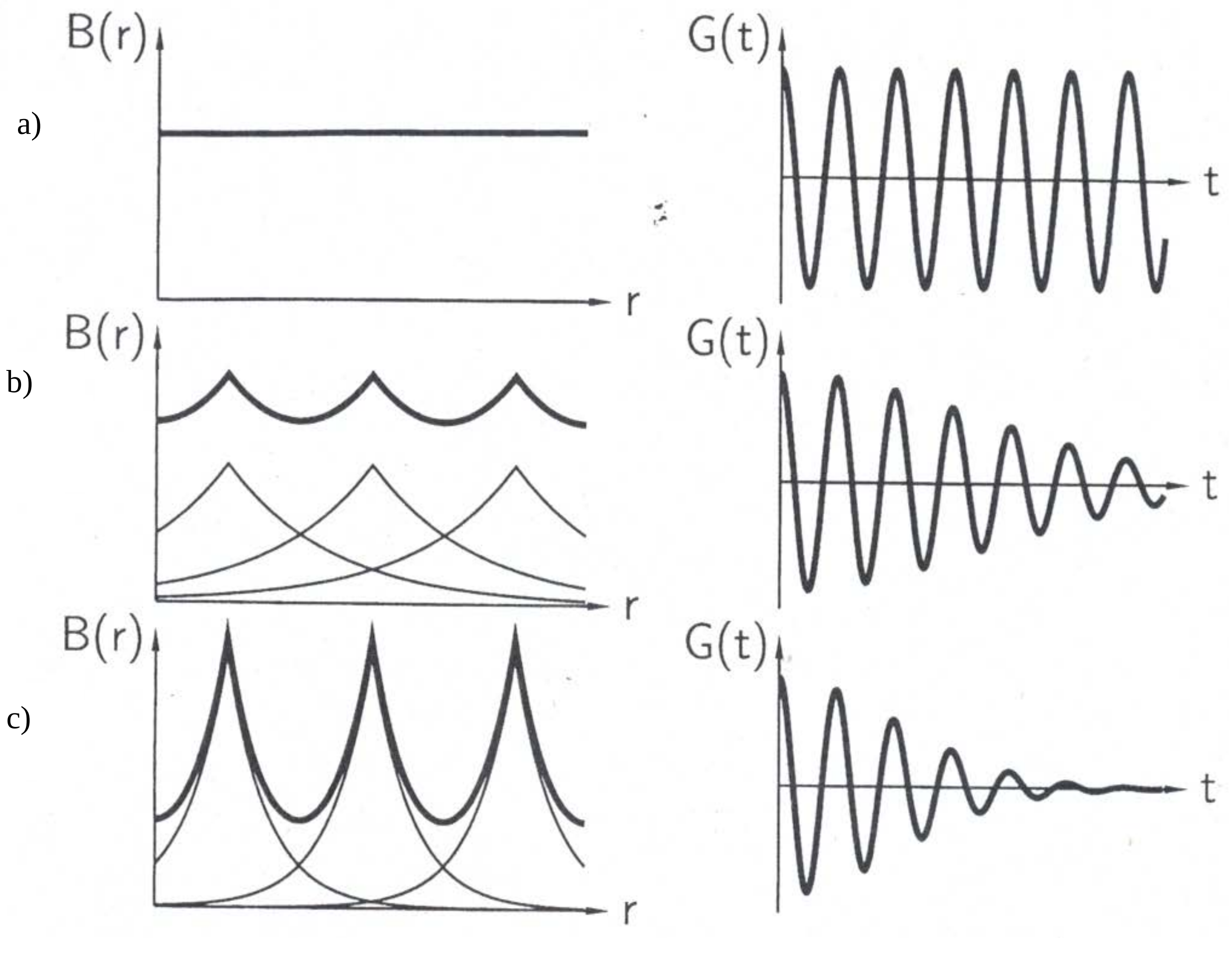

Fig. 7-8: Spatial distribution of fields inside a superconductor (schematically) a) Normal state, b) Vortex state, $T \approx T_c$. c) $T << T_c$. Right: corresponding asymmetry spectra.
From S.J. Blundell, Contemporary Physics **40**, 175-192 (1999).

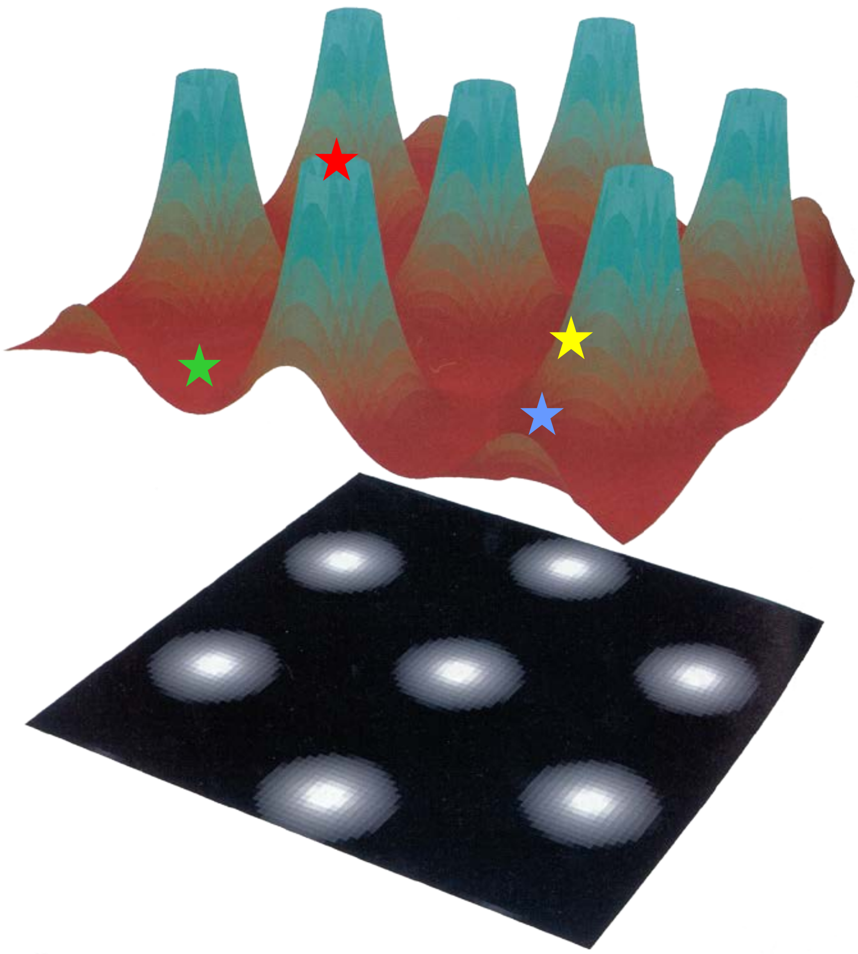

Fig. 7-9: Spatial distribution $B_z(\vec{r})$ of a regular vortex lattice ($\vec{B}_{ext} \parallel \hat{z}$).

The corresponding field distribution $p(B_z)$ is given by

$$p(B_z) = \frac{1}{S}\int_S d^2\vec{r}\ \delta(B_z - B_z(\vec{r}))$$

(S is the surface of the 2D unit cell). The field distribution (and corresponding contour plot in the inset) has the form[2]:

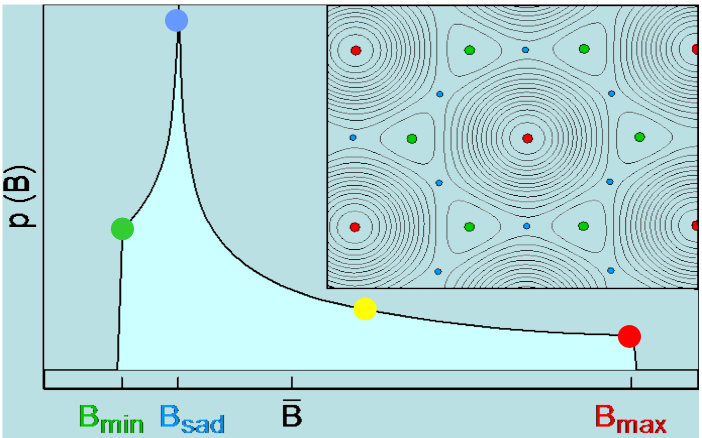

[2] Note that the maximum field (at the center of the vortex) is infinite in the London model. The field profile has been cut here near the flux line center.

The expected μSR signal (TF geometry, $B_{ext} \parallel z$) can be written as (N_μ number of detected muons):

$$P_x(t) = \frac{1}{N_\mu}\sum_{i=1}^{N_\mu}\cos(\gamma_\mu B_i t + \phi)$$
$$P_x(t) = \int p(B)\cos(\gamma_\mu B t + \phi)dB$$

Polarization and p(B) are related via a Fourier transform.

7.2 Second moment of the field distribution of an extreme type II superconductor

The second moment of the field distribution can be calculated explicitely.
Assumptions:
-Ginzburg-Landau parameter κ >>1 (we neglect the extension of the vortex core)
-London model valid (up to ~ $B_{c2}/4$)
-Vortex cores are separated and non-interacting
-Linear superposition of the vortex fields

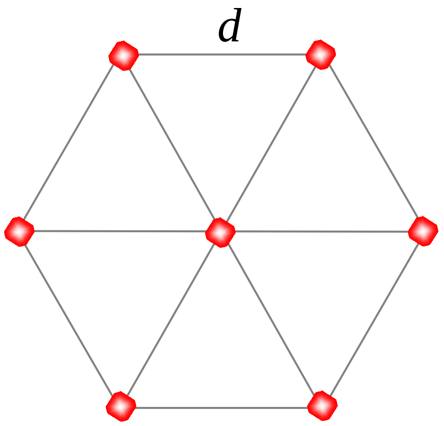

Vortex distance d:

Area of the unit cell containing one vortex: $S = d^2\frac{\sqrt{3}}{2}$

$$\Phi_0 = S < B > \rightarrow d = \sqrt{\frac{2\Phi_0}{< B > \sqrt{3}}}$$

The special field distribution B(r) can be calculated from a modified London equation taking into account the flux source given by the vortices[3]:

$$\vec{B}(\vec{r}) + \lambda^2(\text{rot rot } \vec{B}(\vec{r})) = \Phi_0\sum_n \delta(\vec{r} - \vec{r}_n)\hat{z}$$
$$\vec{B}(\vec{r}) - \lambda^2\Delta\vec{B}(\vec{r}) = \Phi_0\sum_n \delta(\vec{r} - \vec{r}_n)\hat{z} \qquad [7\text{-}4]$$

[3] The left hand side is obtained by applying the rot operation to the Maxwell equation $\text{rot}\vec{B} = \mu_0\vec{j}$ then using the second London equation and $\text{rot}(\text{rot}\vec{B}) = \text{grad div}\vec{B} - \Delta\vec{B}$.

In an ideal vortex state the vectors $\vec{r}_n$ form a periodic two dimensional lattice. Therefore [7-4] can be solved in Fourier space ($\vec{k}$ space):

For an hexagonal lattice:

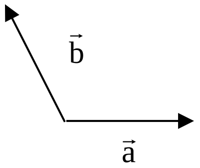

$$|\vec{a}| = |\vec{b}| = d,\ \vec{a} \cdot \vec{b} = \cos 120^\circ$$

Reciprocal vectors:

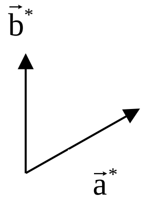

$$\vec{a}^* = 2\pi \frac{\vec{b} \times \vec{c}}{\vec{a} \cdot (\vec{b} \times \vec{c})}, \qquad \vec{b}^* = 2\pi \frac{\vec{c} \times \vec{a}}{\vec{a} \cdot (\vec{b} \times \vec{c})}$$

$$|\vec{a}^*| = \frac{4\pi}{\sqrt{3}d} = |\vec{b}^*|$$

$$\vec{k}_{m,n} = m\vec{a}^* + n\vec{b}^*$$

(also hexagonal symmetry)

$$\vec{B}(\vec{r}) = \sum_{\vec{k}} \vec{b}_k e^{i\vec{k}\vec{r}} \qquad [7\text{-}5]$$

With Fourier components:

$$\vec{b}_{\vec{k}} = \frac{1}{S} \int \vec{B}(\vec{r}) e^{-i\vec{k}\vec{r}} d^2\vec{r}$$

London equation becomes (fields parallel to z-direction):

$$\sum_{\vec{k}} (\vec{b}_{\vec{k}} + \lambda^2 k^2 \vec{b}_{\vec{k}}) e^{i\vec{k}\vec{r}} = \frac{1}{S} \Phi_0 \hat{z} \sum_{\vec{k}} e^{i\vec{k}\vec{r}}$$

We find:

$$\vec{b}_k = \frac{<B>}{1 + k^2\lambda^2} \hat{z} \qquad [7\text{-}6]$$

Where <B> is the (space) averaged internal field ($<B> = N\Phi_0$, $N=1/S$: vortex density).

$$B_z(\vec{r}) = \sum_{\vec{k}} \frac{<B>}{1 + k^2\lambda^2} e^{i\vec{k}\vec{r}}$$

With $b_0 = <B>$ we obtain for the second moment of the field distribution:

$$<\Delta B_z{}^2> = \sum_{\vec{k} \neq 0} |b_{\vec{k}}|^2$$

In a perfect hexagonal lattice:

$$k^2 = k_{m,n}{}^2 = \frac{16\pi^2}{3d^2}(m^2 - mn + n^2) \quad \text{and with } k\lambda >> 1 \ (\langle B\rangle >> B_{c1})$$

$$< \Delta B_z{}^2 >= \frac{3\Phi_0{}^2}{64\pi^4\lambda^4} \sum_{(m,n)\neq(0,0)} \frac{1}{(m^2 - mn + n^2)^2}$$

$$< \Delta B_z{}^2 >= (\frac{0.003710\ \Phi_0^2}{\lambda^4}) \qquad [7\text{-}7]$$

The quantity $< \Delta B^2 >$ is directly related to the magnetic penetration depth λ.

The measurement of the second moment of the field distribution allows therefore to determine the London penetration depth. Note that [7-7] predicts a field width independent of the external field. The formula is valid for small inductions $b \equiv \langle B\rangle/B_{c2} << 1$ and large κ, more precisely in the range $0.13/\kappa^2 << b << 1$ (H. Brandt, Phys. Rev. B**68**, 054506 (2003)).

It holds also[4]:

$$B_{min} - < B > \ \propto \frac{1}{\lambda^2}$$

$$B_{max} - < B > \ \propto \frac{1}{\lambda^2}$$

$$B_{sad} - < B > \ \propto \frac{1}{\lambda^2}$$

[4] About demagnetization in vortex state. The quantities H_i, magnetization M, demagnetization factor N ($0 \le N \le 1$) and mean magnetic flux <B> (i.e. the observed mean internal field) are related to each other by: $H_i = \frac{< B >}{\mu_0} - M = H_{ext} - NM$. Since the μ^+ Knight shift is generally negligible (e.g. in high-T_c materials), the muon spin precession shift is given by: $< B > - \mu_0 H_{ext} = (1 - N)\mu_0 M$ (M<0).

If we cannot neglect the coherence length ξ (radius of the vortex core), we have to introduce in [7-6] a „cutoff" of the terms with k~1/ξ i.e.[5]:

$$\vec{b}_k = \frac{<B>}{1+k^2\lambda^2}\hat{z} \qquad \rightarrow \qquad \vec{b}_k = \frac{<B> e^{-k^2\xi^2}}{1+k^2\lambda^2}\hat{z}$$

(E.H. Brandt, J. Low Temp. Phys. **73**, 355 (1988)).

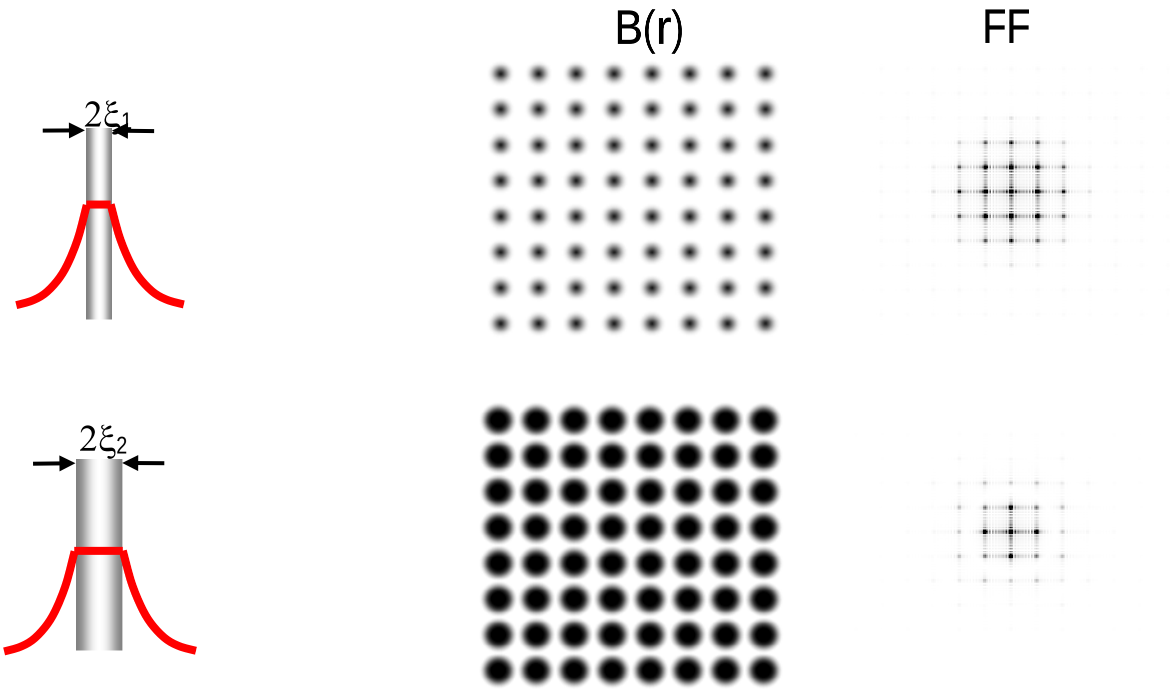

[5] Near b=1 the Abrikosov solution of the linearized Ginzburg-Landau theory yields for all κ values (H. Brandt, Phys. Rev. B **68**, 054506 (2003)):

$$<\Delta B_z{}^2> = \left(\frac{7.52 \cdot 10^{-4}\ \Phi_0^2}{\lambda^4}\right) \frac{\kappa^4(1-b)^2}{(\kappa^2-0.069)^2}$$

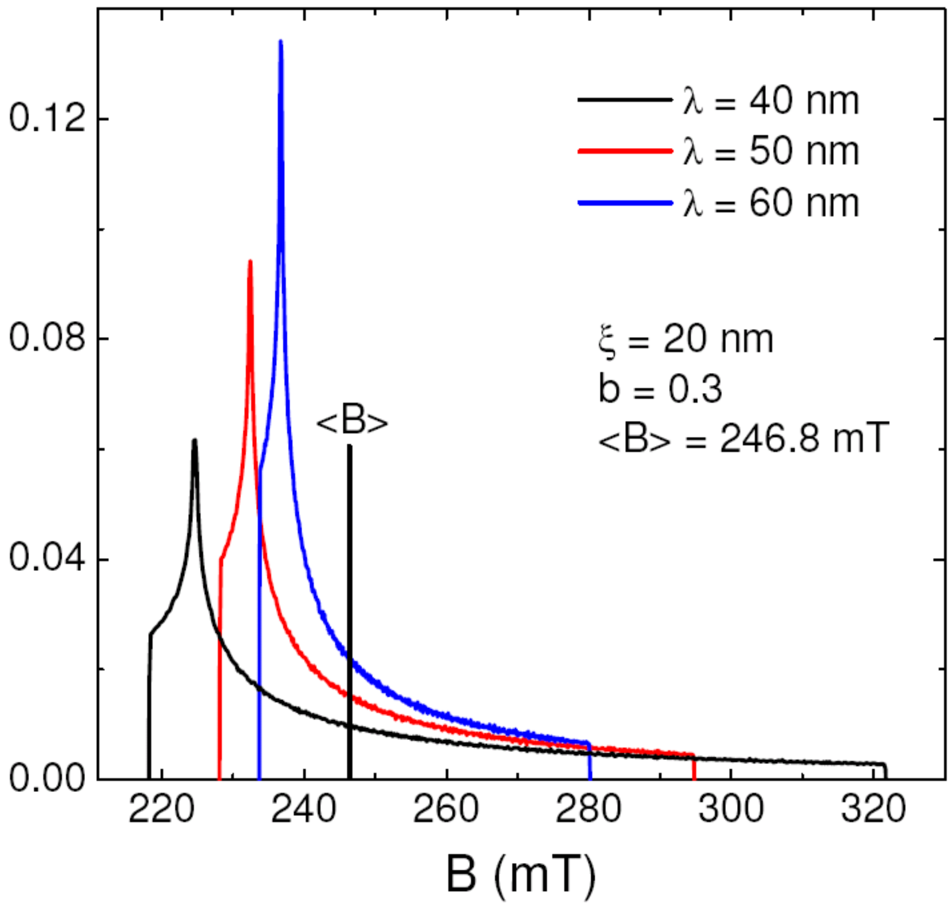

Fig. 7-10: Calculated field distributions. From A. Maisuradze et al., J. Phys.: Condens. Matter **21**, 075701 (2009).

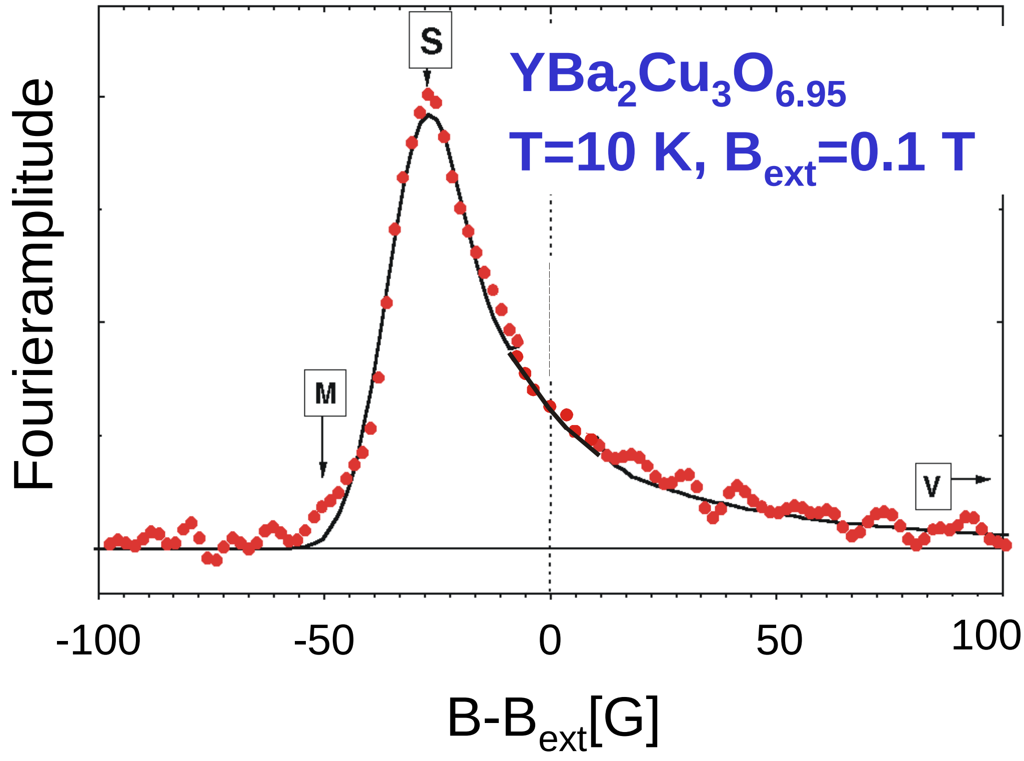

Fig. 7-11: Measured field distribution in YBCO obtained from the Fourier transform of the μSR spectrum.

To determine the magnetic penetration depth the magnetic field is applied above T_c in aTF configuration. Then the temperature is gradually lowered below T_c (field cooling). This way one obtains a regular flux line lattice below T_c ($H_{c1}<H_{ext}<H_{c2}$). In a high-T_c material λ as well as the diamagnetism are anisotropic.
In principle one needs the full field distribution p(B) to determine λ. However, depending on the physical situation the relaxation of the transversal field μSR signal below T_c can be approximated by a Gauss function. In a polycrystalline sample the signal is the integral over all possible orientations of the crystal grains. This leads to a more symmetric p(B), whose Fourier transform (=relaxation function) is closer to a Gaussian function. In this case the second moment of the field distribution can be obtained from the μSR spectrum fitted with a Gaussian relaxation (which implicitly implies that p(B) is Gaussian) and the field width and the magnetic penetration depth are directly related to the Gaussian relaxation rate σ_{sc}:

$$\sigma_{sc}^2 = \gamma_\mu^2 < \Delta B^2 >= \gamma_\mu^2 (< B^2 > - < B >^2) \qquad [7\text{-}8]$$

To obtain σ_{sc} one has generally to subtract from the measured σ the temperature independent contribution of the broadening due to the nuclear moments σ_n, which is obtained by a measurement above T_c:

$$\sigma_{sc}(T) = \sqrt{\sigma^2(T) - \sigma_n^2}$$

Assuming eq. [7-7] and $\frac{\sigma_{sc}}{\gamma_\mu} = \sqrt{<\Delta B^2>}$ there is a simple numerical relationship between the muon depolarisation rate σ_{sc} and the superconducting penetration depth λ namely $\lambda = \frac{327.5}{\sqrt{\sigma_{sc}}}$, σ_{sc} in μs^{-1}, λ in nm. A Gaussian fit is only sensitive to the central part of the field distribution of a non-Gaussian distribution. This is sometimes taken into account empirically by using the expression $\lambda = \frac{270.0}{\sqrt{\sigma_{sc}}}$, σ_{sc} in μs^{-1}, λ in nm.

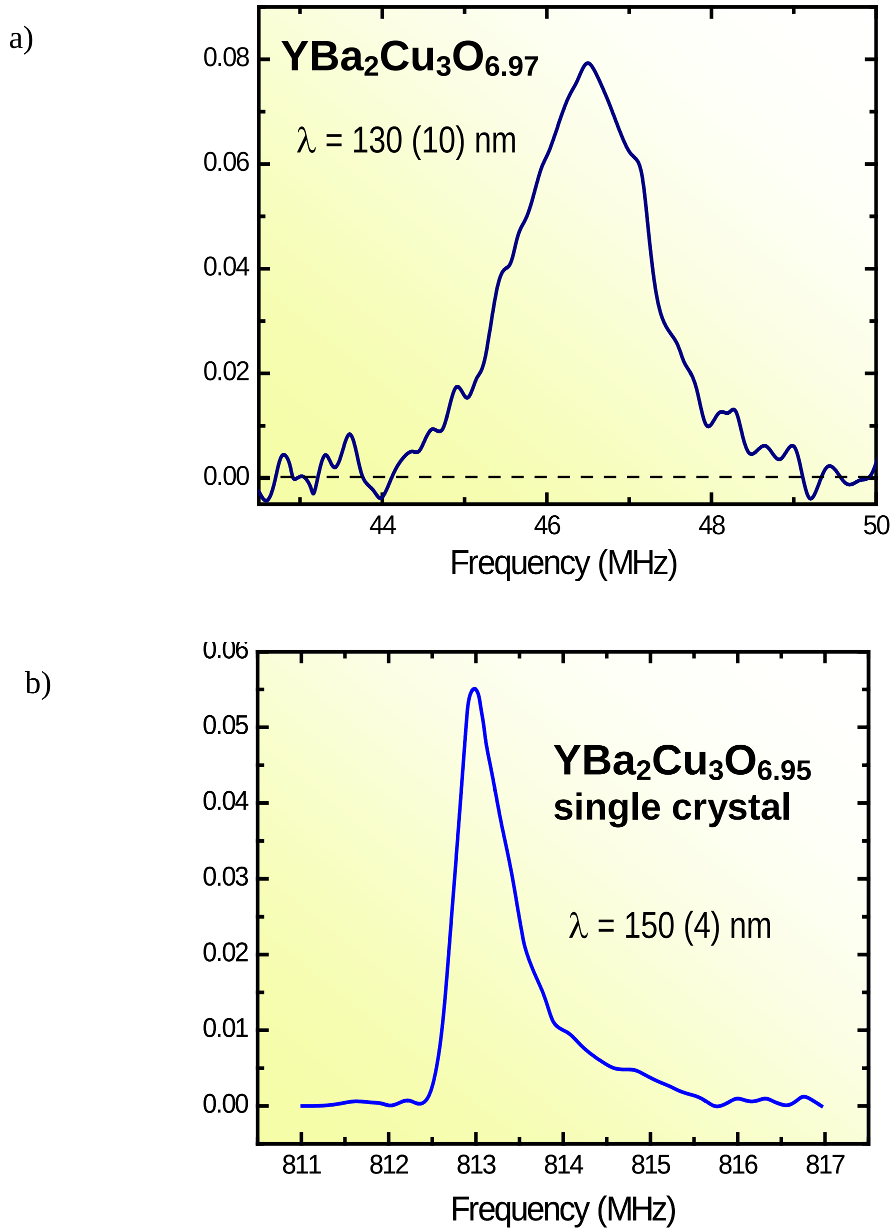

Fig. 7-12: Comparison of p(B) (a) in a polycrystalline YBCO sample (from B. Pümpin et al., Phys. Rev. B **42**, 8019 (1990)) and (b) in a single crystal (from J. Sonier et al., PRL **83**, 4156 (1999)).

7.3 Field dependence

If the applied magnetic field is not small with respect to B_{c2} the decrease of the intervortex distance may lead to a decrease of the width of the internal field distribution. Also the vortex core where the superconducting order parameter is suppressed cannot be neglected any more (remember $B_{c2} = \frac{\Phi_0}{2\pi\xi_{GL}^2}$, Φ_0 flux quantum). In this case, the expected field dependence of the second moment of the field distributions has been calculated within the Ginzburg-Landau model (E. H. Brandt, Phys. Rev. B **68**, 054506 (2003)) and a modified London Model with a Gaussian cut off to take into account the finite size of the vortex core (E. H. Brandt, Phys. Rev. B **37**, 2349 (1988)).The two expressions differ essentially in the higher order corrections to the linear field dependence ($b \equiv \langle B\rangle/B_{c2}$), generally $\langle B\rangle \approx B_{ext}$, see [5]). Calculations based on Ginzburg -Landau can be well approximated by:

$$\sigma_{sc}\ [\mu s^{-1}] = 4.854\cdot 10^4 (1-b)\left[1+1.21(1-\sqrt{b})^3\right]\frac{1}{\lambda[nm]^2} \qquad [7\text{-}9]$$

whereas the modified London model gives:

$$\sigma_{sc}\ [\mu s^{-1}] = 4.846\cdot 10^4 (1-b)\sqrt{1+3.9(1-b^2)}\,\frac{1}{\lambda[nm]^2} \qquad [7\text{-}10]$$

An example of such a behavior in the iron pnictide $RbFe_2As_2$ (T_c=2.52 K) is shown. (Z. (Shermadini et al., Phys. Rev. B **82**, 144527 (2010)).

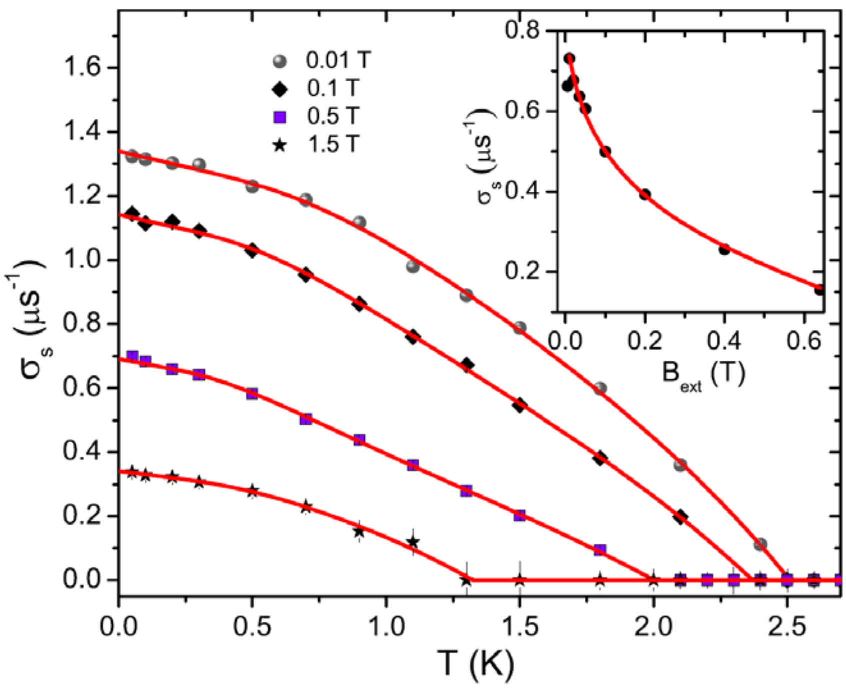

Fig. 7-13: Temperature dependence of the depolarization rate σ_{sc} due to the FLL in $RbFe_2As_2$ and obtained in fields of 1.5, 0.5, 0.1, and 0.01 T (lines are guides to the eyes). Inset: field dependence of σ_{sc} obtained at 1.6 K and analyzed using the Eq. [7-9].

By analyzing at each temperature (not too close to T_c), the field dependence of σ_{sc} with Eq. [7-9] one obtains $\lambda(T)$ and $B_{c2}(T)$. From the temperature dependence of $1/\lambda(T)^2$ we obtain information about the superconducting gap of the material (see section 7.6).

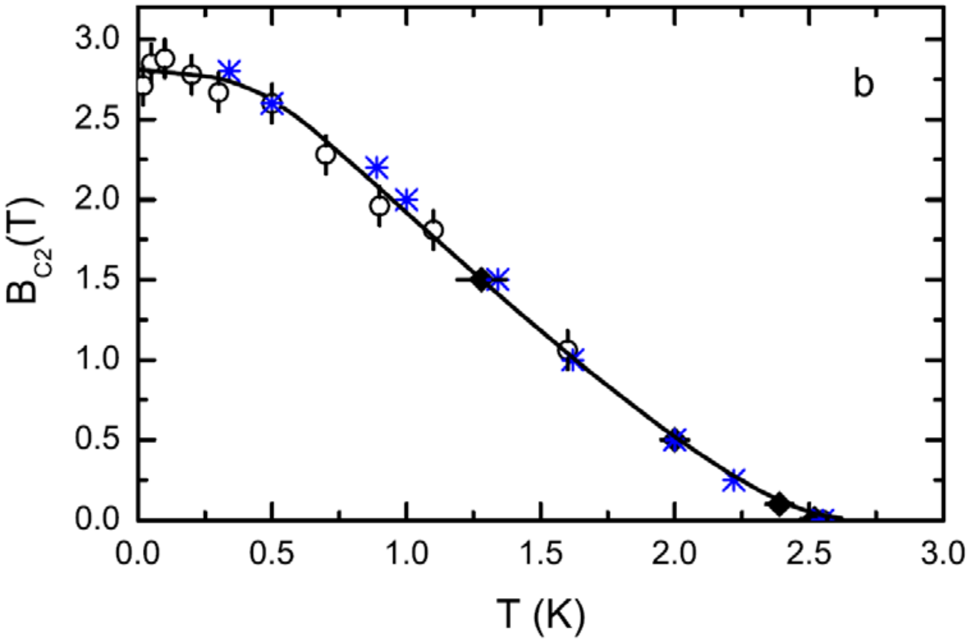

Fig. 7-14: Upper critical field for $RbFe_2As_2$. The open circles are obtained by analyzing the field dependence of σ_{sc} using Eq. [7-9]. The diamonds are the value obtained by analyzing the temperature dependence of σ_{sc}. The stars correspond to the complete disappearance of the resistivity in field. The line is a guide to the eyes.

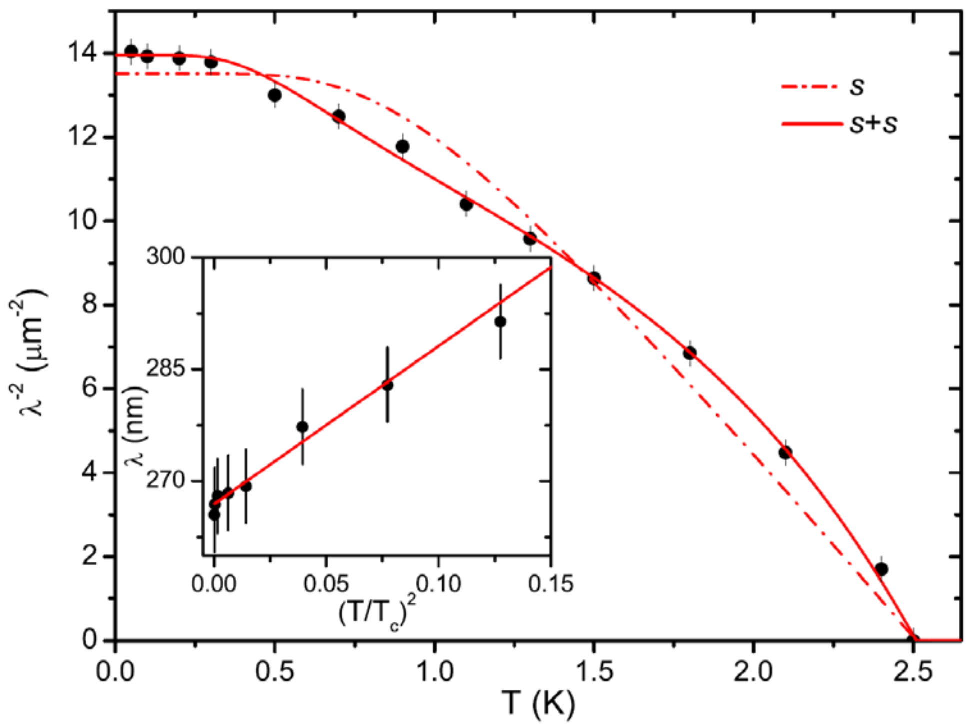

Fig. 7-15: Magnetic penetration depth as a function of temperature obtained with Eq. [7-9]. Above 0.5 K only the values measured in a field of 0.01 T are plotted. The red dashed line corresponds to a BCS *s*-wave gap symmetry whereas the solid one represents a fit using a two-gap *s*+*s* model (see Section 7-6). The inset exhibits the penetration depth as a function of $(T/T_c)^2$.

7.4 Uemura relation: Correlation between T_c und σ_{sc} (Phys. Rev. Lett. **66**, 2665 (1991))

Since the discovery of superconductivity in the copper oxide materials there has been a considerable effort to find universal trends and correlations amongst physical quantities to find a clue to the origin of the superconductivity. One of the earliest patterns that emerged was the linear scaling of the Gauss relaxation σ_{sc} with the superconducting transition temperature (T_c). This is referred to as the Uemura relation and works reasonably well for the underdoped materials.

The linear relation between T_c und σ_{sc} (Fig. 7-16) implies a direct correlation between T_c and the superfluid density $\rho_s \equiv \frac{n_s}{m^*}$ since $\sigma_{sc} \propto \frac{1}{\lambda^2} \propto \frac{n_s}{m^*}$. The magnetic penetration depth in cuprates is anisotropic. For polycrystalline samples λ is an average of λ_c and λ_{ab} (ab = CuO_2 planes). For $\lambda_c >> \lambda_{ab}$, σ_{sc} is only sensitive to λ_{ab} (W. Barford and J.M.F. Gunn, Physica 153-155C, 691 (1988)).

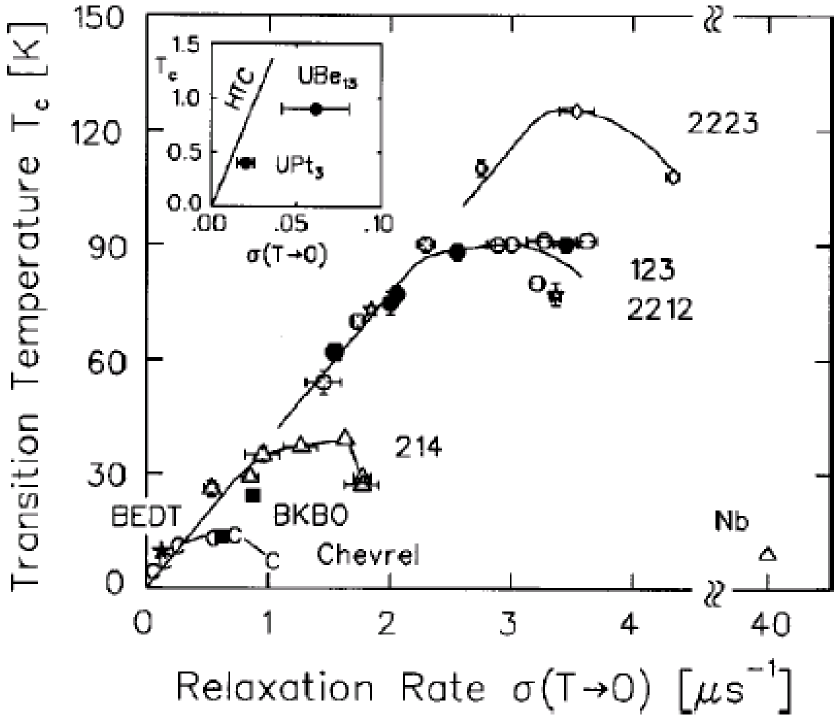

Fig. 7-16: T_c vs muon depolarization rate $\sigma(0)$ in (i) the high-temperature superconductors: $YBa_2Cu_3O_{7-\delta}$ (123), $La_{2-x}Sr_xCuO_4$ (214), $Bi_2Sr_2CaCu_2O_8$, and $Tl_{0.5}Pb_{0.5}Sr_2CaCu_2O_7$ (2212), and $Bi_{2-x}Pb_xSr_2Ca_2Cu_3O_{10}$, $Tl_2Ba_2Ca_2Cu_3O_{10}$, and $Tl_{0.5}Pb_{0.5}Sr_2Ca_2Cu_3O_9$ (2223) [note: hole doping increases with increasing $\sigma(0)$]; (ii) $Ba_{1-x}K_xBiO_3$ (BKBO); (iii) the Chevrel-phase systems $LaMo_6Se_8$, $LaMo_6S_8$, and $PbMo_6S_8$; (iv) the organic superconductor (BEDT-TTF)$_2$Cu(SCN)$_2$; (v) the conventional superconductor Nb; and (vi) the heavy-fermion superconductors UPt_3 and UBe_{13}. From Uemura *et al.*, 1991.

Such a correlation is not consistent with conventional weak coupling BCS theory for phonon coupled superconductors, where

$$T_c \cong \frac{2\hbar\omega_D}{k_B} e^{-\frac{2}{VD(E_F)}} \qquad [7\text{-}11]$$

ω_D = Debye frequency (phonon coupling)
$D(E_F)$ = Density of states at Fermi level E_F
V= effective attractive pair potential (→ Cooper pair).

In [7-11] T_c is proportional to ω_D and not simply related to n_s.

Fig. 7-16 indicates that these „unconventional“ superconductors belong to a different class of materials than that of the previously known “conventional” superconductors (such as Nb, Al,..).
If the energy scale of the pairing is of the order of the Fermi energy, one would expect:

$$T_c \propto T_F \qquad [7\text{-}12]$$

For a 2D electron gas the Fermi energy is given by:

$$E_F = k_B T_F = \frac{\hbar^2 \pi n_{s-2d}}{m^*} \qquad [7\text{-}13]$$

High- T_c superconductors are to large extent two dimensional, since the CuO_2 planes contain most of the supercarriers (electrons or holes).

One obtains:

$$T_c \propto \frac{n}{m^*}$$

A linear relationship between critical temperature and superfluid density is also obtained if T_c is primarily determined by long range phase ordering.

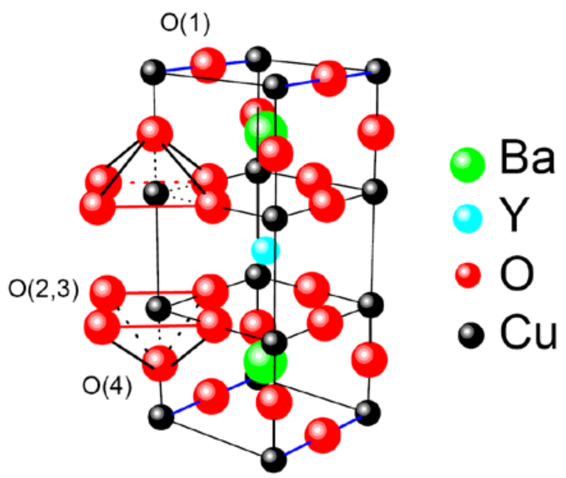

Fig. 7-17: Crystal structure of $YBa_2Cu_3O_{7-\delta}$ with 2 CuO_2 planes and CuO chains as charge reservoir.

μSR measurements of the penetration depth in the vortex state and the Uemura plot are used to classify superconductors (e.g. the newly discovered Fe based superconductors).

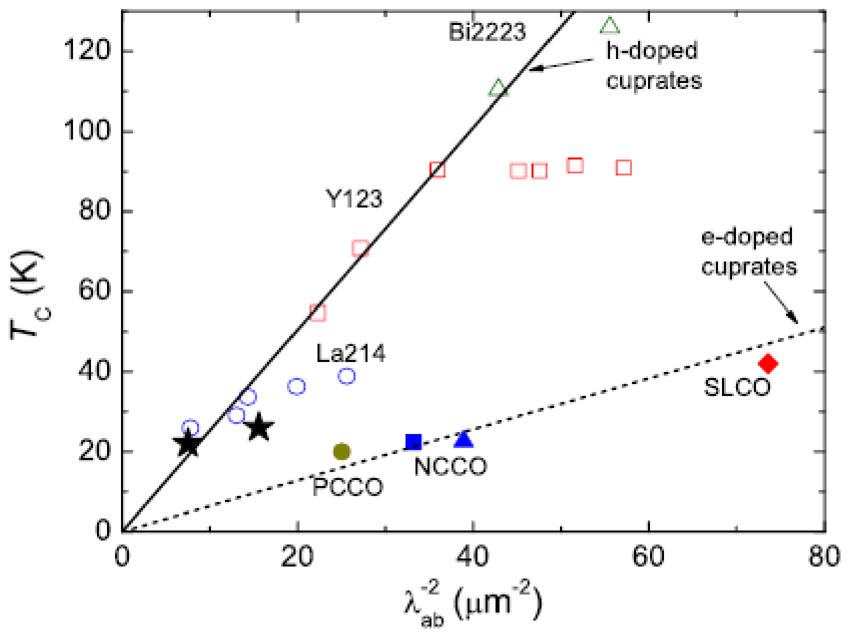

Fig. 7-18: Uemura plot for hole and electron doped high T_c cuprates and for the $LaFeAsO_{1-x}F_x$ pnictide (★) (from H. Luetkens et al., Phys. Rev. Lett. **101**, 097009 (2008)).

7.5 Measurement of the anisotropy of the magnetic penetration depth

Measurement with oriented YBCO single crystals. The theory predicts:

$$\sigma_{sc}(\vartheta) = \frac{\text{const}}{\lambda_{ab}\lambda_c}\sqrt{\sin^2\vartheta + \frac{\lambda_c{}^2}{\lambda_{ab}{}^2}\cos^2\vartheta} \qquad [7\text{-}14]$$

In this equation, λ_{ab} and λ_c are the principal values of the London penetration depth for a superconductor with uniaxial asymmetry: λ_{ab} and λ_c are determined by superconducting screening currents flowing parallel and perpendicular to the CuO_2 planes, respectively.
ϑ is the angle between external field and c-axis.
From the measurement one can determine the anisotropy parameter γ.

$$\gamma^2 = \frac{\lambda_c^2}{\lambda_{ab}^2} = \frac{m_c^*}{m_{ab}^*} \qquad [7\text{-}15]$$

ϑ = 0, H_{ext} || c-axis. Shielding currents flow in (a,b) plane
ϑ = 90, $H_{ext} \perp$ c-axis. Shielding currents flow along c and a (or b) axis

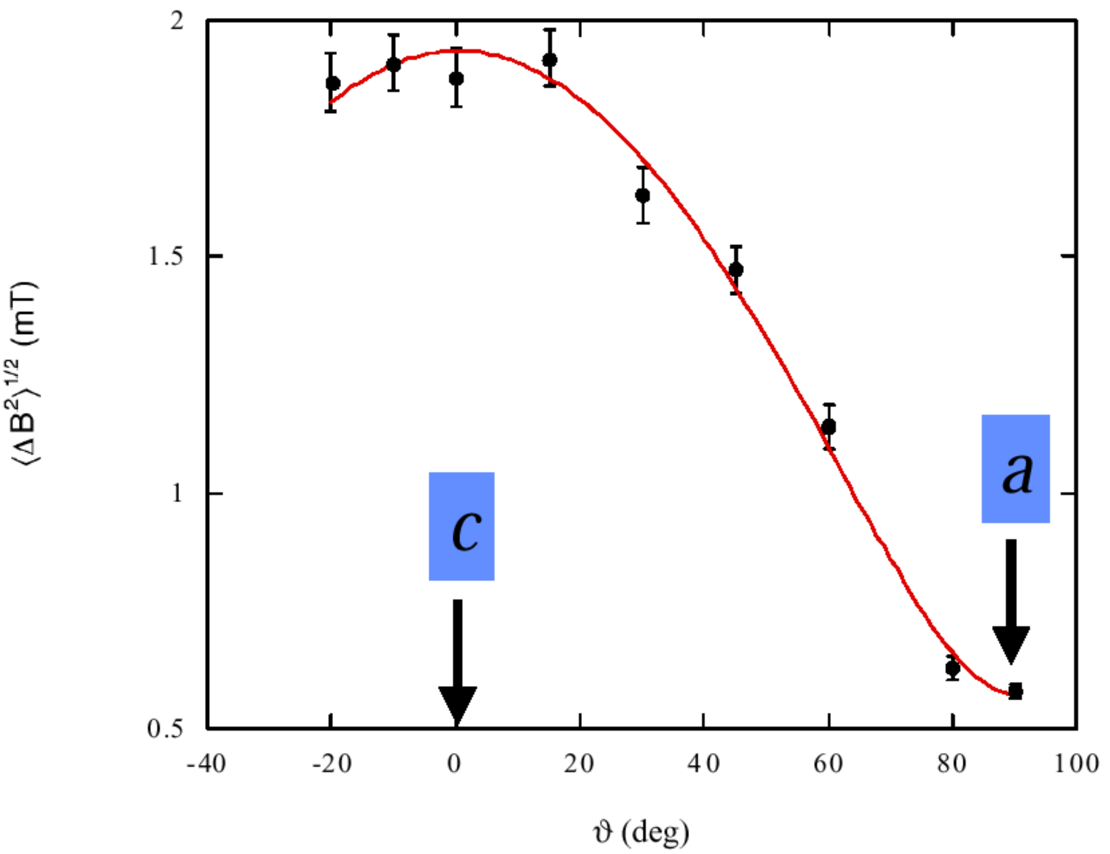

Fig. 7-19: Angular dependence of the second moment of the field distribution in YBCO single crystal. The curve is a fit to [7-14], γ=3.9(6). (E. M. Forgan et al., Hyperfine Interact. **63**, 71 (1990))

7.6 Temperature dependence of $\lambda(T)$ and of the superconducting carrier density

From a µSR measurement we obtain $\sigma \propto \frac{1}{\lambda^2} \propto \frac{n_s}{m^*}$. The temperature dependence of n_s contains information on the superconducting gap $\Delta(T)$. Therefore, an accurate measurement of the temperature dependence of λ provides information on the superconducting gap such as value at T=0 K and symmetry.

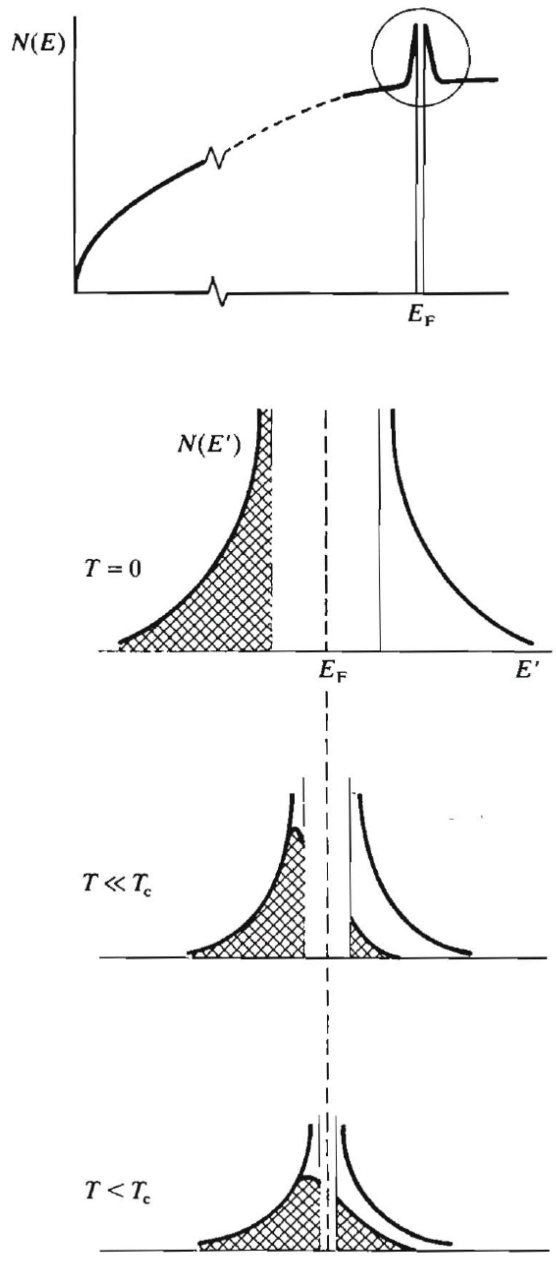

Fig. 7-20: Density of states and state population as a function of temperature in an s-wave superconductor, showing the opening of the superconducting gap with temperature.

By taking into account the thermal population of the quasiparticle excitations of the Cooper pairs (Bogoliubov quasiparticles) BCS theory predicts:

$$n_s(T) = n_s(0)\left(1 - \frac{2}{k_B T}\int_0^{\infty} f(\varepsilon,T)\left[1 - f(\varepsilon,T)\right]d\varepsilon\right) \qquad [7\text{-}16]$$

$$f(\varepsilon,T) = \frac{1}{1 + e^{\frac{\sqrt{\varepsilon^2+\Delta(T)^2}}{k_B T}}} \qquad [7\text{-}17]$$

where ε is the energy of the normal state electrons measured from the Fermi level ($E = \sqrt{\varepsilon^2 + \Delta(T)^2}$ energy of the quasiparticles measured from Fermi level).

For isotropic s-wave pairing (as in the case of conventional BCS superconductor) and $T \ll T_c$:

$$n_s(T) = n_s(0)\left(1 - \sqrt{\frac{2\pi\Delta(0)}{k_B T}}\exp\left[-\Delta(0)/k_B T\right]\right) \qquad [7\text{-}18]$$

and

$$\lambda(T) = \lambda(0)\left(1 + \sqrt{\frac{\pi\Delta(0)}{2k_B T}}\exp\left[-\Delta(0)/k_B T\right]\right) \qquad [7\text{-}19]$$

(B. Mühlschlegel, Z. Phys. 155, 313 (1959)).

The wave function of the two paired electrons can be written as the product of a space and a spin part: $\Psi(\vec{r}_1, s_1, \vec{r}_2, s_2) = \phi(\vec{r}_1, \vec{r}_2)\chi(s_1, s_2)$.

The wave function must be antisymmetric with respect to particle exchange.
If the spin state is a singlet S=0, $\chi = \frac{1}{\sqrt{2}}(\left|\uparrow\downarrow\right\rangle - \left|\downarrow\uparrow\right\rangle)$ the space part must be even, e.g.. s-wave (l=0) or d-wave (l=2). Conventional BCS superconductors are so-called s-wave superconductor, whereas high-T_c cuprate superconductors have d-wave symmetry. This is observable in a measurement of the temperature dependence of the magnetic penetration depth.
Instead of eq. [7-16] we have for a d-wave superconductor:

$$n_s(T) = n_s(0)\left(1 - \frac{1}{\pi k_B T}\int_0^{2\pi}\int_0^{\infty} f(\varepsilon,T)\left[1 - f(\varepsilon,T)\right]d\varphi d\varepsilon\right) \qquad [7\text{-}20]$$

with:

$$f(\varepsilon, T) = \frac{1}{1 + e^{\frac{\sqrt{\varepsilon^2 + [\Delta(T)\cos(2\varphi)]^2}}{k_B T}}}$$

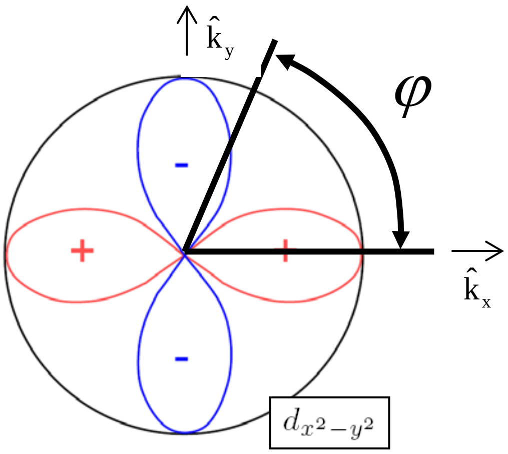

Gap function $\Delta(\mathbf{k})$. It has lower symmetry than the Fermi surface

As the gap disappears along some directions of the Fermi surface (“nodes”), extremely-low-energy quasiparticles excitations (and therefore significant pair-breaking) may occur at very low temperature.

This is reflected in a more pronounced temperature dependence of λ than for s-wave pairing. Remembering that $\lambda = \sqrt{\frac{m^*}{\mu_0 e^2 n_s}}$ one gets for $T \ll T_c$ a linear T-dependence:

$$\lambda(T) = \lambda(0)\left(1 + \frac{\ln 2 k_B T}{\Delta(0)}\right) \qquad [7\text{-}21]$$

(Hirschfeld and Goldenfeld, Phys. Rev. **B48**, 4219 (1993)).

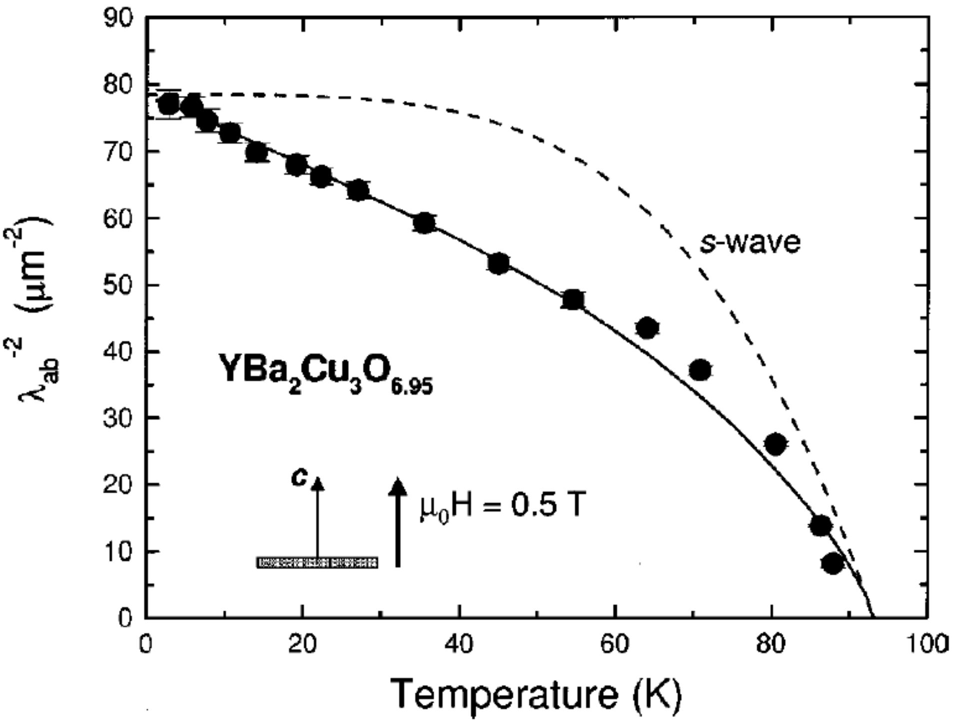

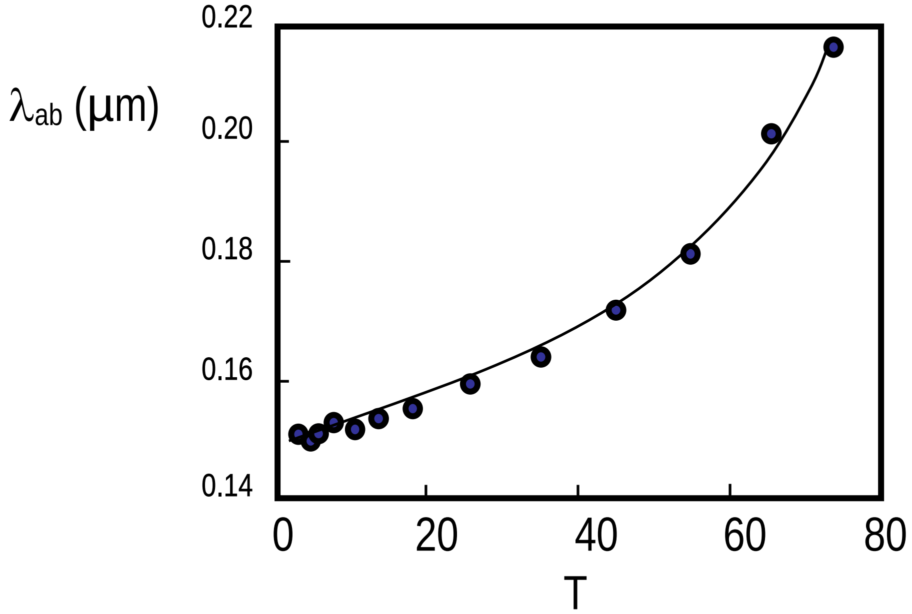

Fig. 7-21: Top: Temperature dependence of λ_{ab}^{-2} in a $YBa_2Cu_3O_{6.95}$ single crystal. Measurement of $\Delta\lambda_{ab}$ with microwave absorption normalized to the μSR measurements. Dashed line: temperature dependence for an s-wave superconductor. (μSR measurement: J. Sonier, Phys. Rev. Lett., **72**, 744 (1994), microwave measurement: W.N. Hardy, Phys. Rev. Lett **70**, 3999 (1993)). Bottom: $\lambda_{ab}(T)$ showing the linear dependence at low temperatures.

7.7 Melting of the flux line lattice

The vortex state of a High-T_c superconductor represents a unique state of the solid that can be compared with a crystal and its lattice. The “lattice constant” of the vortex state can be changed by the external field and the temperature in a wide range.
Especially in a HT_c superconductor, the combination of extreme anisotropy, thermal fluctuations (important since T_c is large) and material defects lead to a complex behavior, which can be described by a corresponding phase diagram with phase transitions solid-liquid or ordered-disordered.

μSR measurements were the first microscopic investigations that demonstrated the melting of the flux line lattice.

The vortex state is characterized by the moments of the field distribution.

$$\alpha = \frac{<\Delta B^3>^{1/3}}{<\Delta B^2>^{1/2}} \qquad <\Delta B^n> = \int_0^\infty (B-<B>)^n p(B)dB \qquad [7\text{-}22]$$

α represents a measure of the asymmetry of p(B).

In the extreme anisotropic HT_c-superconductor such as $Bi_{2.15}Sr_{1.85}CaCu_2O_{8+d}$ (T_c=84 K) following is observed (S.L. Lee et al. Phys. Rev. Lett. 71, 3862 (1993)):

a) Until 54K and H_{ext}=45.4 mT the expected distribution is found.
b) Increasing the temperature to 54 K (H_{ext}= 45.4 mT) leads to a dramatic change of p(B). α jumps abruptly to a negative value. This behavior is interpreted as melting of the flux line lattice (Fig. 7-19).
c) Increasing the external field at constant temperature (in a field cooling procedure) one observes above a critical field another phase transition (Fig. 7-22), which is not so drastic as the previous one and which is also characterized by a change of α. This behavior is interpreted as a transition to a less ordered solid state, with a dimensionality change from 3D to 2D (formation of so-called pancakes vortices).

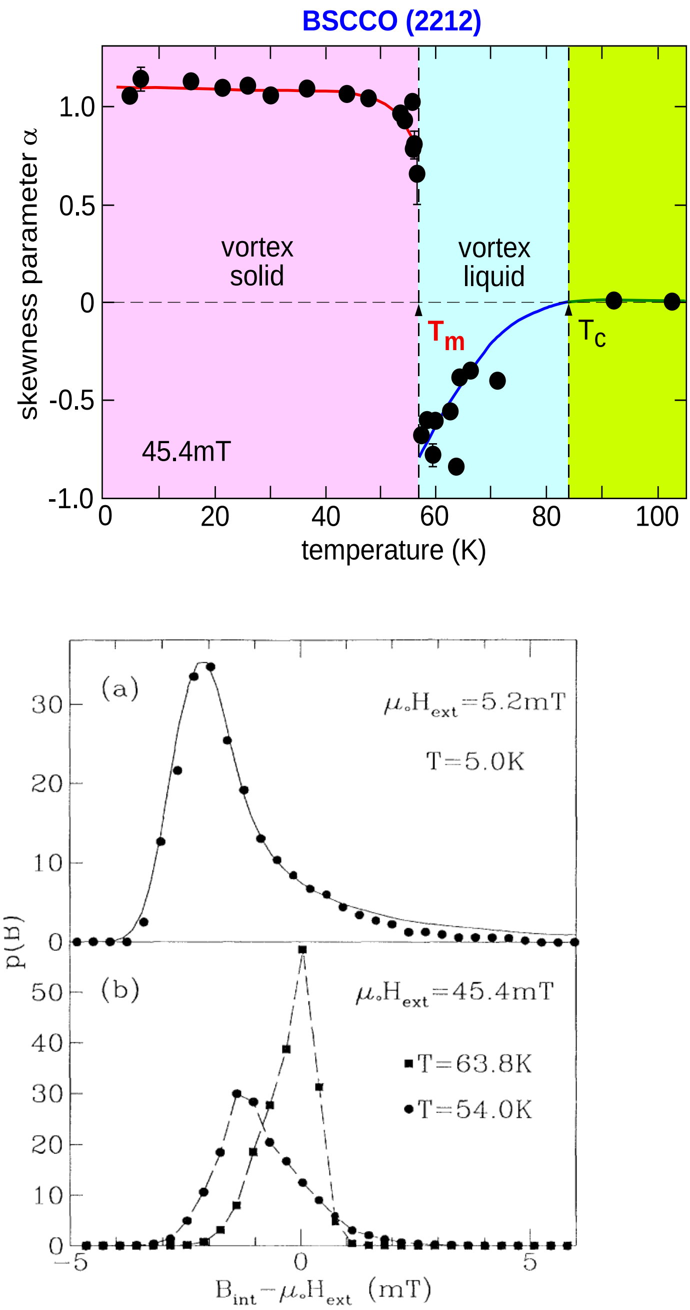

Fig. 7-22: Phase diagram of $Bi_{2.15}Sr_{1.85}CaCu_2O_{8+d}$ and field distribution measured in different states (5 K solid, 63.8 K liquid).

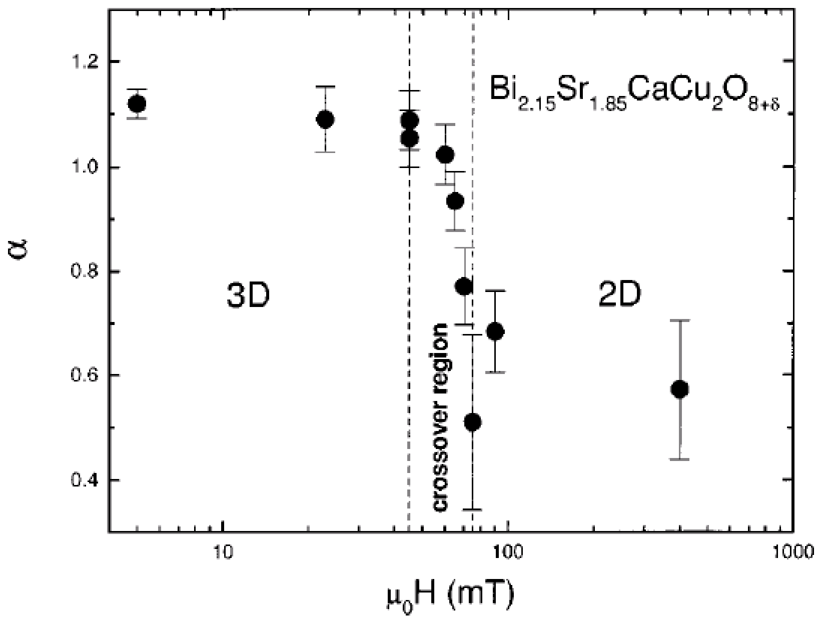

Fig. 7-23:Magnetic-field dependence of the skewness parameter α in single crystal $Bi_{2.15}Sr_{1.85}CaCu_2O_{8+\delta}$ after field cooling at T=5K. The sharp drop in α at μ_0H ~ 50 mT is attributed to a 3D to 2D crossover in the vortex lattice. From S.L. Lee et al. Phys. Rev. Lett. **71**, 3862 (1993).

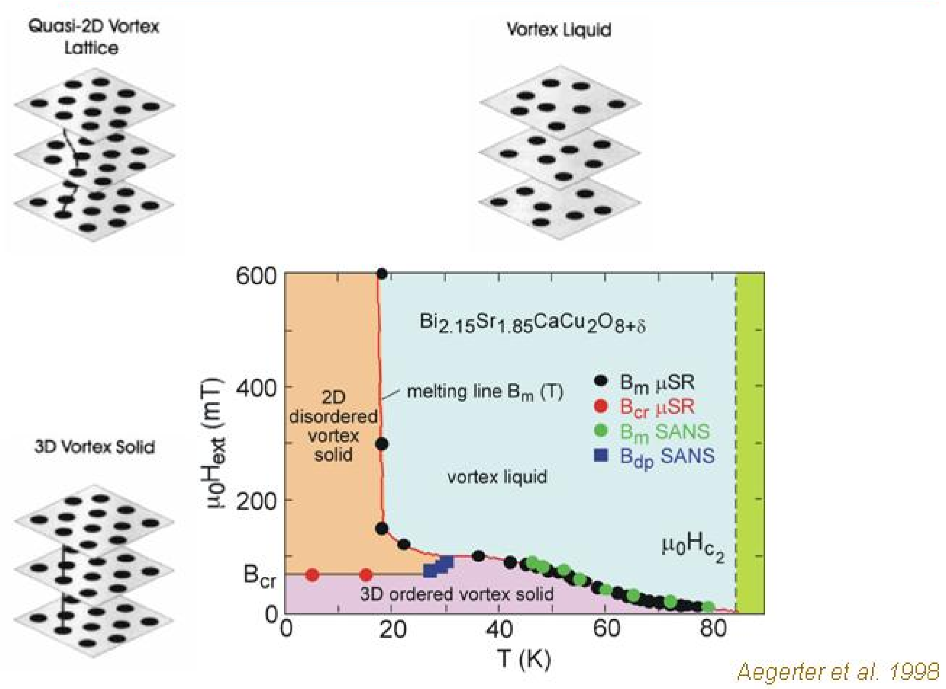

Fig. 7-24: Phase diagram of the vortex state of BSCCO, determined from μSR and small angle neutron scattering experiments (SANS).

7.8 Coexistence of magnetism and superconductivity

Example : $YBa_2Cu_3O_{6+x}$ (ref. S. Sanna et al., Phys. Rev. Lett., **93** 207001 (2004))
(x Oxygen give h=x/6 holes per Cu planar atom)
Coexistence of magnetic (AF order and correlations) and superconducting phases can be investigated by a combination of ZF and TF (in vortex state) measurements.

ZF:

$$A_z(t) = a_L G_z(t) + a_T G_x(t)\cos(\gamma_\mu |\vec{B}_1| t)$$

$$a_L + a_T = a_{ZF}$$

$\vec{B}_1$: local field

for a homogeneous magnetic (polycrystalline) sample:

$$\frac{a_L}{a_{ZF}} = \frac{1}{3} \quad \text{and} \quad \frac{a_T}{a_{ZF}} = \frac{2}{3}$$

if only part of the sample is magnetic:

$$\frac{a_L}{a_{ZF}} > \frac{1}{3} \quad \text{and} \quad \frac{a_T}{a_{ZF}} < \frac{2}{3}$$

The volume fraction is given by:

$$f_{AF} = \frac{3}{2}\frac{a_T}{a_{ZF}} = \frac{3}{2}\left(1 - \frac{a_L}{a_{ZF}}\right)$$

In the vortex state

$$A_x(t) = a_{TF} G_x(t)\cos(\gamma_\mu B_\mu t)$$

$$G_x(t) = e^{-\frac{(\sigma_{sc}^2 + \sigma_n^2)t^2}{2}}$$

$B_\mu = \mu_0 H(1+\chi)$ and $\chi<1$

σ_n is the contribution of the nuclear moments

The volume fraction is given by:

$f_{SC} = \frac{a_{TF}}{a_0}$ where a_0 is obtained at $T>T_c$

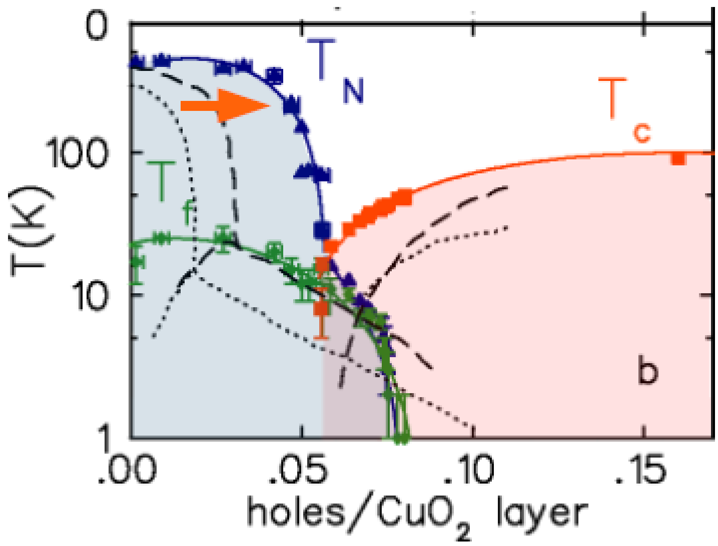

<u>Fig. 7-25</u>: Phase diagram of $YBa_2Cu_3O_{6+x}$. Solid lines are guides to the eye, dashed $Y_{1-y}Ca_yBa_2Cu_3O_{6+x}$) and dotted ($La_{2-x}Sr_xCuO_4$) lines from C. Niedermayer et al., PRL **80**, 3843 (1998).

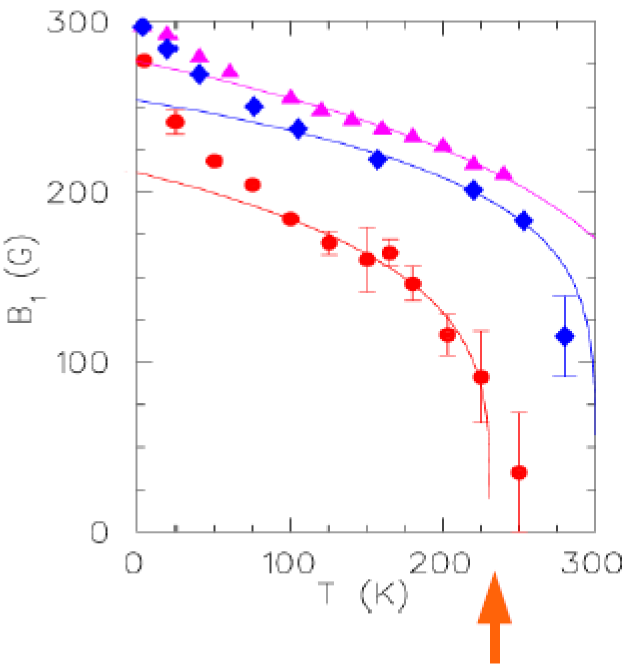

<u>Fig. 7-26</u>: Local field vs T at different doping x.

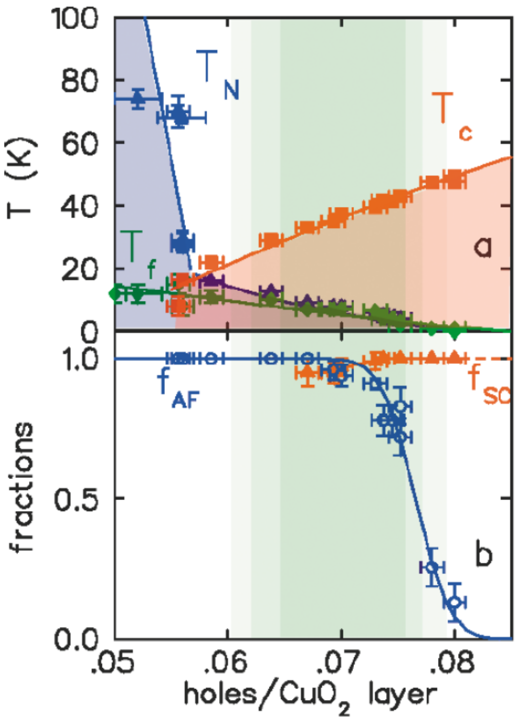

Fig. 7-27: (a) magnetic transition temperatures ▲ from a_L/a_{ZF}, ◆ from $1/T_1$ and sc critical temperature T_c, vs hole concentration *h*; three samples show a distinct T_N>T_f.
(b) Muon volume fractions vs *h*: AF (○ at T=0 K) and SC (▲, for T_f<T<T_c). Lines in (a), (b) are guides to the eye.

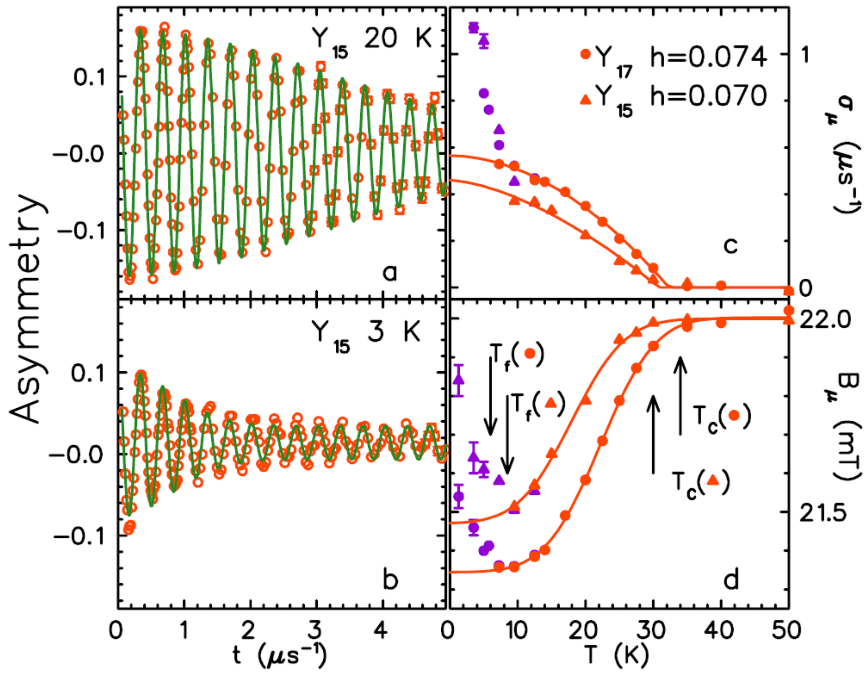

Fig. 7-28: TF μSR data ($\mu_o H$ = 22 mT). Asymmetry (a) for T_f <T = 20 K<T_c and (b) for T = 3K < T_f in sample Y15; solid curves are best fits to a Gaussian damped precession. (c) Relaxation rate σ_{sc} (here labelled σ_μ) and (d) internal field B_μ from the best fits for samples Y15 and Y17.

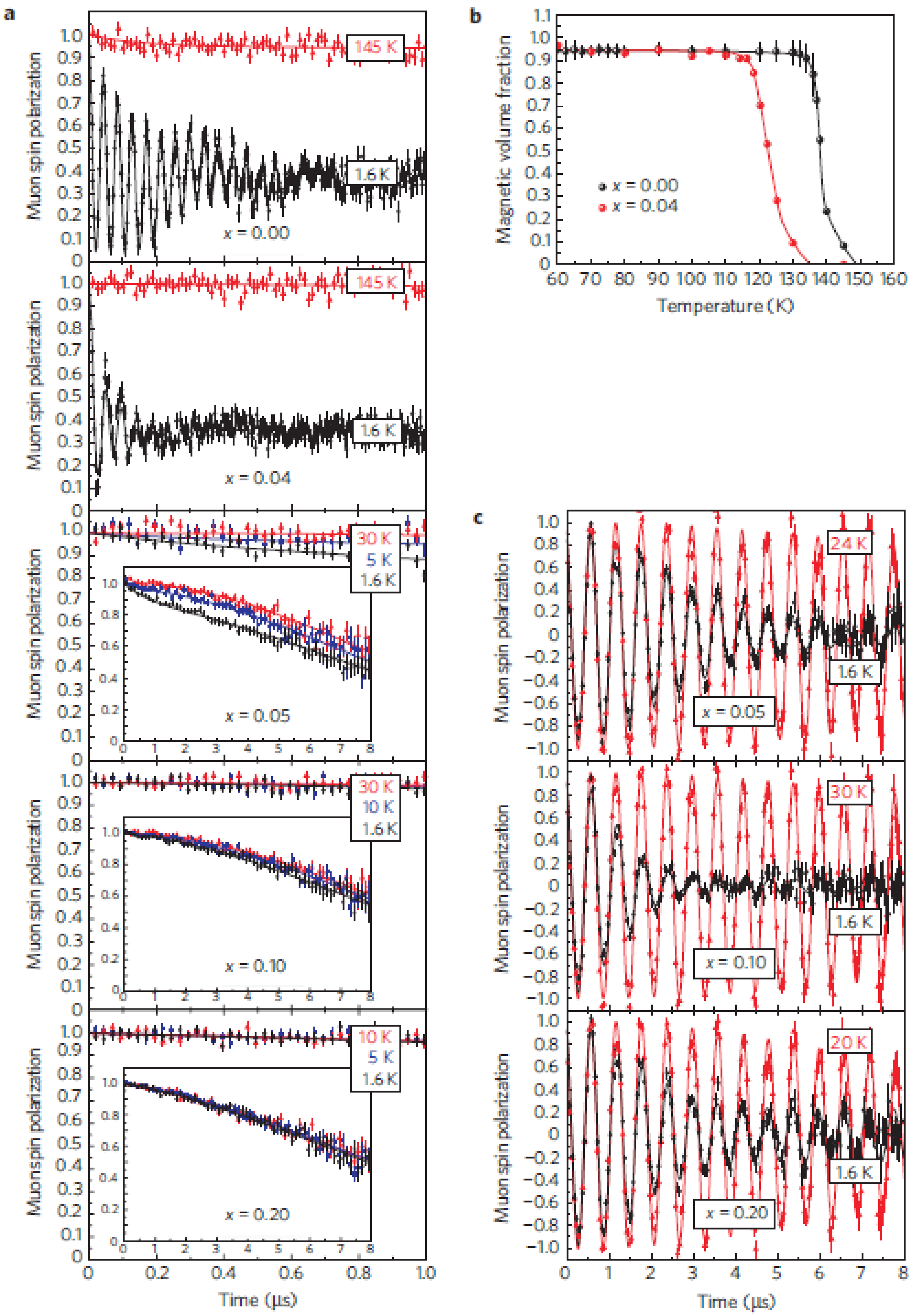

Fig. 7-29: a) Typical zero-field µSR spectra. Only for x≤0.04 a spontaneous muon spin precession indicative of long-range-ordered magnetism is observed. For x≥0.05 a paramagnetic signal is observed down to the lowest temperatures. For *x*=0.05 a weak electronic relaxation typical for diluted static magnetism is detected below 5 K in <30% of the signal (visible on the long timescale in the inset). For x≥0.075 the µSR data prove that no static magnetism is present. b), Temperature dependence of the magnetic volume fraction for *x*=0 and 0.04. Both samples show a transition to a 100% magnetic volume fraction. The ~ 5%

non-magnetic signal is attributed to muons stopping in the sample holder. c) Typical transverse-field μSR spectra measured in an external field of 0.07 T (for clarity shown in a rotating reference frame with frequency 7.8 MHz). The additional Gaussian relaxation due to the formation of the flux-line lattice in the superconducting state is clearly observed below T_C. Note that for x=0.20 a signal fraction of 15% does not show this additional relaxation, indicating the presence of a non-superconducting volume fraction (from H. Luetkens et al., Nature Materials **8**, 305 - 309 (2009)).

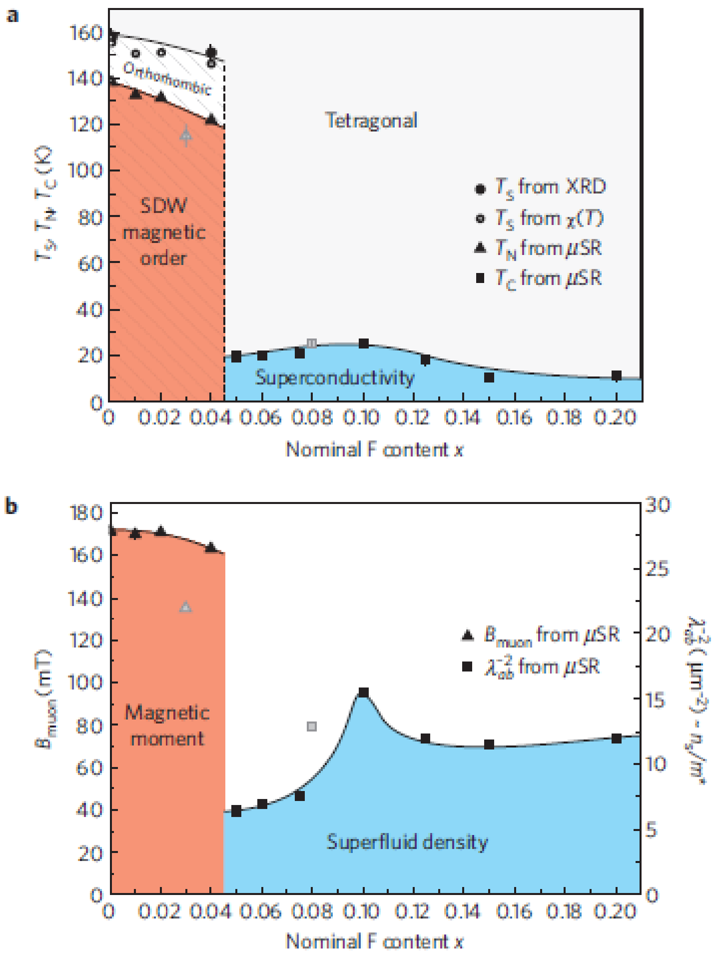

Fig. 7-30: a) The doping dependence of the magnetic and superconducting transition temperatures determined from the μSR experiments. Also shown are the tetragonal-to-orthorhombic structural transition temperatures T_S determined directly from X-ray diffraction and from susceptibility measurements, which show a kink and subsequent strong reduction below T_S. b) The doping dependence of the low-temperature saturation value of the magnetic order parameter $B_{muon}(T\rightarrow 0)$ and of the superfluid density n_s/m^* measured through $1/\lambda_{ab}^2(T\rightarrow 0)$ in transverse-field μSR experiments. The grey data points at x=0.03 and 0.08 are taken from another work. The error bars indicate one standard deviation.